JGR Planets

RESEARCH ARTICLE
10.1029/2025JE009077

Effect of Magnetic Field Configuration on Interchange Convection in the Jovian Inner Magnetosphere

Yuxian Wang[1,2], Xiaocheng Guo[1,2], Michel Blanc[3], Hui Li[1,2], and Chi Wang[1,2]

[1]State Key Laboratory of Solar Activity and Space Weather, National Space Science Center, Chinese Academy of Sciences, Beijing, China, [2]College of Earth and Planetary Sciences, University of Chinese Academy of Sciences, Beijing, China, [3]Institut de Recherche en Astrophysique et Planétologie (CNRS / University Toulouse III – CNES), Toulouse, France

Abstract The interchange instability drives the concurrent cold iogenic plasma convection and energetic particle injection in the Jovian inner magnetosphere. We use an improved Rice Convection model—Jupiter to simulate plasma transport under a more realistic magnetic field configuration, which is determined by magnetodisc currents. A series of runs were conducted to parametrically investigate the effect of the magnetic field configuration on the convection system. Simulation results show that the azimuthal magnetodisc current significantly influences plasma convection. The asymmetry in the longitudinal distribution of the azimuthal current strongly enhances the longitudinal asymmetry in the initial stage of magnetospheric evolution. The instability and associated plasma radial velocity tend to increase with increasing current intensity. By the quasi-steady stage, the longitude-averaged mass flux remains similar and is largely unaffected by variations in current intensity. The longitudinal asymmetry also becomes less pronounced during this phase. The radial current has little effect on the convection system, while the magnetic tilt angle can slightly reduce the instability.

Plain Language Summary The outward transport of cold plasma originating from Jupiter's moon Io and the inward injection of hot plasma are commonly observed in Jupiter's inner magnetosphere. This transport process is driven by the so-called interchange instability, a phenomenon similar to the Rayleigh-Taylor instability seen in fluid dynamics. The longitudinal asymmetry of the Jovian magnetosphere may come from external factors such as solar wind compression or internal factors such as the ionosphere and the Io plasma source. In this study, we used an improved inner magnetosphere model to simulate plasma convection under a more realistic magnetic field configuration that includes longitudinal asymmetry. Our findings indicate that the magnetic field configuration significantly affects the plasma transport at Jupiter.

Key Points:

- We simulate plasma convection under a realistic magnetic field configuration using an improved Jovian inner magnetosphere model
- The magnetic field configuration significantly influences plasma convection at Jupiter
- The azimuthal magnetodisc current is the dominant factor in the magnetic field's effect on plasma transport

Correspondence to:

X. Guo and C. Wang,
xcguo@spaceweather.ac.cn;
cw@spaceweather.ac.cn

Citation:

Wang, Y., Guo, X., Blanc, M., Li, H., & Wang, C. (2025). Effect of magnetic field configuration on interchange convection in the Jovian inner magnetosphere. *Journal of Geophysical Research: Planets*, *130*, e2025JE009077. https://doi.org/10.1029/2025JE009077

Received 12 MAR 2025
Accepted 4 JUL 2025

1. Introduction

The dynamics of the Jovian magnetosphere are primarily governed by a combination of solar wind interaction and the planet's rapid rotation (spin period: ~10 hr) (e.g., Bagenal et al., 2017; Bolton et al., 2015). In deep regions of the magnetosphere, far from the magnetopause, global mass and energy circulation are mainly controlled by the planetary rotation along with the dominant internal mass source, Io (Bagenal et al., 2017; Krupp et al., 2004; Vasyliunas, 1983).

In the inner magnetosphere close to the planet (e.g., $L < 20\ R_J$, $1\ R_J = 71{,}492$ km), iogenic plasma largely rigidly corotates with Jupiter and gradually spirals outward. Outward transport is facilitated by the so-called interchange instability, a process driven by centrifugal forces (e.g., Mauk et al., 2002; Vasyliūnas & Pontius, 2007; Wang et al., 2024). A direct consequence of this instability is the interchange convection, which involves the outward displacement of mass-loaded magnetic flux tubes and the inward motion of returning flux tubes containing hot, tenuous plasma from outside regions. The latter process is often termed energetic injection (Dumont et al., 2018; Haggerty et al., 2019; Louarn et al., 2014; Mauk et al., 2002). This mechanism plays a crucial role in the plasma transport within the Jovian inner magnetosphere (Bolton et al., 2015).

Observational evidence of the interchange convection and associated plasma injection at Jupiter has been provided by a combination of in situ measurements (e.g., Bolton et al., 1997; Daly et al., 2023, 2024; Kivelson et al., 1997; Louarn et al., 2014; Mauk et al., 1997) and imaging data (e.g., Dumont et al., 2014, 2018; Grodent et al., 2018; Haggerty et al., 2019; Mauk et al., 2002). An interchange event is typically characterized by a rapid increase in magnetic field strength and sudden changes in particle flux. These events are sometimes accompanied by the detection of various types of waves (e.g., Daly et al., 2023, 2024). Similar processes have also been

identified in Saturn's magnetosphere, another rotationally dominated planetary magnetosphere (e.g., Burch et al., 2005; Menietti et al., 2008; Radioti et al., 2009; Yin et al., 2025).

Theoretical calculations demonstrate that the linear stage of interchange instability is primarily influenced by the plasma distribution, the ionospheric Pedersen conductance, the magnetic field and energetic particles (André & Ferrière, 2007; Huang & Hill, 1991; Pontius, 1997; Southwood & Kivelson, 1989; Vasyliūnas & Pontius, 2007). These predictions were validated through Rice Convection Model (RCM)-based simulations (Wang et al., 2023; Wu et al., 2007; Yang et al., 1994). Additional factors, including inhomogeneous Hall conductance, Io source rate, injection site location and energetic plasma density, were also examined during the non-linear stage of the instability (Wang et al., 2023, 2024). This interchange convection can also be reproduced by global magneto-hydrodynamic (MHD) models (e.g., Chen et al., 2023; Feng et al., 2023; Schok et al., 2023; Tanaka et al., 2023).

The averaged Jovian magnetic field in a typical state of the inner magnetosphere can be well described by a combination of the planet's intrinsic magnetic field and the contributions from the magnetodisc current sheet (Connerney et al., 2020, 2022). Longitudinal asymmetry in the Jovian magnetosphere is evident in observations, including particles (Krupp et al., 2001; Yuan et al., 2024), large-scale structures (Khurana, 2001; Liu et al., 2023, 2024) and auroral emissions (Grodent, 2015). The longitudinal asymmetry comprises two components: one corotates with the planet, and the other is a local time asymmetry fixed in the inertial frame. The corotating component may be influenced by factors such as the asymmetric Io plasma torus, the non-dipole terms in the planet's intrinsic magnetic field, and the ionosphere (e.g., Al Saati et al., 2022; Bolton et al., 2015), while the local time asymmetry could result from solar wind compressions (Krupp et al., 2004).

Since previous RCM simulations and analyses (e.g., Wang et al., 2023, 2024) used a spin-aligned magnetic dipole to represent the Jovian inner magnetosphere, the impact of magnetic field configuration on plasma convection remains unclear. In this study, we improve the model by employing a more realistic magnetic field configuration to better simulate Jupiter's plasma convection.

The paper is organized as follows. Section 2 describes the model settings. Sections 3 and 4, respectively, present our main simulation results and their discussion. Finally, Section 5 summarizes the key findings and presents our conclusions.

2. Model Description

The RCM-Jupiter code has been successfully used to investigate the interchange convection of cold iogenic plasma and energetic particle injection in the Jovian inner magnetosphere (Wang et al., 2023, 2024). To represent the energy distribution of trapped electrons and ions, their population is represented as the superposition of multiple individual populations of charged particles sharing the same energy (adiabatic) invariant $|\lambda| = E \cdot V^{2/3}$ (Toffoletto et al., 2003), where E is the particle kinetic energy, and V is the flux tube volume. Then, our code, a two-dimensional (2D) multifluid model, simulates the bounce-averaged plasma drifts in a prescribed electric and magnetic field. Each fluid is defined by λ and flux tube content $\eta = \int ndz/B$, which is the number of particles contained per unit magnetic flux (n denotes the number density, and B is the magnetic field).

The RCM logic is based on a corotation enforcement current system, which comprises the magnetodisc current, ionospheric current and FACs connecting the magnetosphere and ionosphere. The plasma population in the Jovian inner magnetosphere is represented by 41 fluids, including the cold oxygen ions (cold O^+, $k = 1$), 20 energies of O^+ ($k = 2$–21), and 20 energies of electrons ($k = 22$–41). The energy of energetic particles at $L = 10\ R_J$ varies from 0.1 to 1,500 keV. A more detailed description of the model logic, Io torus model, energetic plasma and ionospheric conductance model can be found in Wang et al. (2023, 2024). Here, we only introduce the magnetic field setups involved in this study.

2.1. Magnetic Field Model

The magnetic field configuration is one of the key elements in the RCM logic (see Figure 1 in Wang et al., 2023). In situ measurements such as the ones performed by Juno suggest that the real magnetic field at Jupiter becomes increasingly longitude asymmetric, non-dipole, and more stretched at greater radial distances (L) within the Jovian inner magnetosphere (Bagenal et al., 2017; Connerney et al., 2020, 2022). Therefore, in this study,

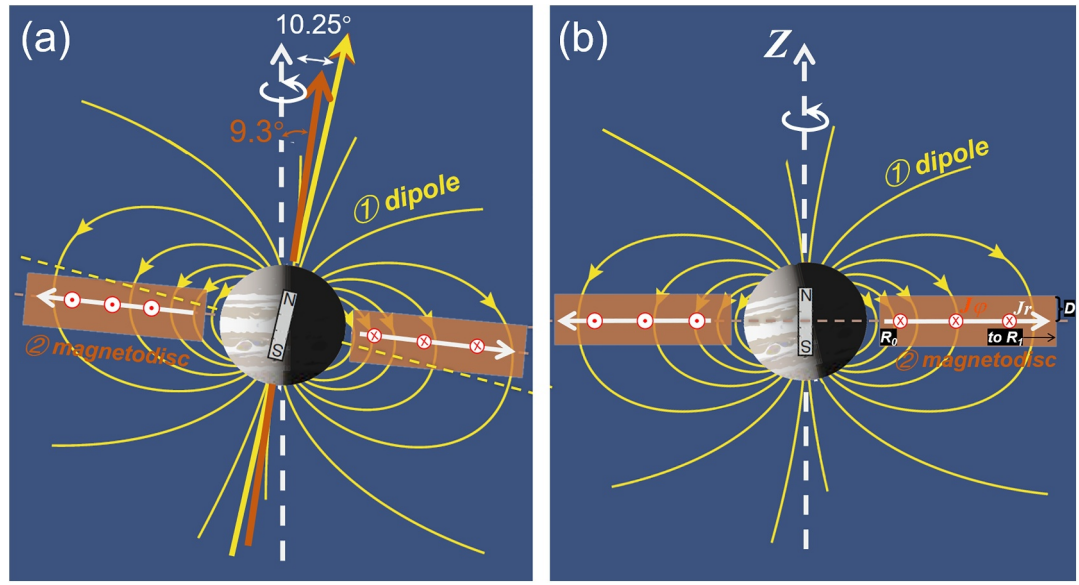

Figure 1. Schematic illustration of the configuration of the intrinsic magnetic field and the magnetodisc current. (a) The realistic dipole field with a tilt angle of 10.25° as described by the JRM33 model (in yellow), and the magnetodisc with a tilt angle of 9.3° from the CON20 model (in orange). (b) The non-tilted magnetic field configuration employed in this study. R_0, R_1, and D are typical parameters defining the current sheet as described by the CON20 model. The dots/crosses enclosed by red circles denote the azimuthal currents J_φ, whereas the white arrows indicate the radial current J_r.

different from previous works (Liu & Hill, 2012; Wang et al., 2023, 2024; Wu et al., 2007), we use a more realistic magnetic field model instead of a simplified, non-tilted magnetic dipole.

As shown in Figure 1a, the static magnetic field ($\boldsymbol{B}$) in Jupiter's inner magnetosphere ($L < 20\ R_J$) can be well described by a combination of the intrinsic magnetic field ($\boldsymbol{B_0}$) model (e.g., JRM33, Connerney et al., 2022) and the magnetodisc current model ($\boldsymbol{B_I}$) (e.g., CON20, Connerney et al., 2020) derived from Juno data, that is, $\boldsymbol{B} = \boldsymbol{B_0} + \boldsymbol{B_I}$. Specifically, the JRM33 model is a degree 18 spherical harmonic model of Jupiter's planetary magnetic field. Its degree 1 coefficients describe a dipole with a moment of 4.177 Gauss and a tilt angle $\theta_{\text{tilt}} = 10.25°$ relative to the rotational axis. The CON20 model represents the magnetic field contributed by the magnetodisc current located near the magnetic equatorial plane with a tilt angle of 9.3°. The magnetodisc current is mainly composed of an eastward azimuthal ("ring") current J_φ and secondarily by an outward radial current J_r. Specifically, the azimuthal current contributes to the deflection of the poloidal magnetic field, while the radial current constitutes a component of the magnetosphere-ionosphere coupling current system, leading to an azimuthal magnetic field perturbation (Connerney et al., 2020). It should be noted that these two models are static and represent the average state of the Jovian inner magnetosphere.

Note that the RCM assumes a north-south symmetry. Therefore, in this study, we neglect the tilt angle between the magnetic axis and the rotational axis, and only retain the dipole components of the intrinsic magnetic field (see Figure 1b). As a result, the consequential magnetic field can be calculated by incorporating the non-tilted dipole field from the JRM33 model and contributions from the CON20 model. Using Juno's magnetic field data, Connerney et al. (2020) constrained the magnetodisc model parameters as follows: the inner radius $R_0 = 7.8\ R_J$, outer radius $R_1 = 51.4\ R_J$, the half thickness $D = 3.6\ R_J$, the intensity of J_φ is defined by $\mu_0 I_0/2 = 139.6$ nT, and J_r intensity is set as $I_R = 16.7$ MA. We note that the current densities are given by $J_\varphi = I_0/\rho$ and $J_r = I_R/(4\pi\rho D)$, where ρ denotes the distance to the magnetic axis (Connerney et al., 2020; Wilson et al., 2023). To investigate the effect of magnetic field configuration on the convection system, we perform a series of runs with different magnetodisc current intensities, that is, $\mu_0 I_0/2$ and I_R.

2.2. Model Settings for All Runs

We start each simulation run from an initially empty magnetosphere until the magnetosphere reaches a quasi-steady state. Similar to our previous work (Wang et al., 2024), we use a relatively low ionospheric Pedersen

conductance $\Sigma_P = 0.2\ S$ and a high Io source rate of 2,000 kg/s to achieve a faster evolution of the magnetosphere. These values are reasonable compared to observations (Al Saati et al., 2022; Bagenal & Delamere, 2011; Wang et al., 2021).

To investigate the effect of magnetic field configuration on the convection system, runs 1–4 adopt different uniformly longitudinally distributed J_φ intensities. Runs 5 and 6 use a longitude asymmetric J_φ in the form of $\mu_0 I_0 = \frac{(\mu_0 I_0)_{\min}+(\mu_0 I_0)_{\max}}{2} + \frac{(\mu_0 I_0)_{\min}-(\mu_0 I_0)_{\max}}{2}\cos(\varphi)$. Such asymmetric distribution of J_φ is artificially prescribed to mimic the longitudinally asymmetric Jovian inner magnetosphere. As mentioned in Section 1, this asymmetry corotates with Jupiter and may result from factors such as the asymmetric Io torus or from processes that corotate with the planet, such as a magnetic dipolarization (e.g., Yao et al., 2020).

Given that Jupiter's magnetic tilt angle θ_{tilt} is 10.25° for the dipole and 9.3° for the magnetodisc (Figure 1a), run 7 is designed to evaluate the effect of θ_{tilt} on convection. The centrifugal equator, defined as the farthest point along a magnetic flux tube from the rotational axis, tends to align with the magnetic equator rather than the rotational equator in the Jovian inner magnetosphere (Moncuquet et al., 2002; Phipps & Bagenal, 2021). Therefore, we can reasonably assume that the plasmasheet concentrates near the magnetic equator in this study. Consequently, the Z-axis of the RCM (see Figure 1b) should be aligned with the magnetic axis due to the fundamental assumption of north-south symmetry as mentioned above. As a result, the equivalent spin angular velocity reduces to $\Omega_J \cdot \cos(\theta_{\text{tilt}})$. The perpendicular component $\Omega_J \cdot \sin(\theta_{\text{tilt}})$ is neglected, although it may slightly displace the plasmasheet from the magnetic equator. Ω_J is Jupiter's angular velocity. More details of these simulation runs are described in Section 3.

3. Simulation Results

In this Section, we first present simulation results from run 5, describing the full evolution of plasma convection starting from an initially empty magnetosphere. This case represents a typical case featuring a longitudinally asymmetric magnetic field configuration. Then, we discuss the effect of the magnetic field configuration on the convection system, including magnetodisc currents (i.e., J_φ and J_r) and the magnetic tilt angle. All the results shown in this study are presented in Jupiter's corotating frame. Note that the highest-energy O^+ ions ($k = 21$, referred to as high-energy O^+ hereafter) and electrons ($k = 41$, referred to as high-energy electrons) are selected as representative cases for the analysis of interchange convection. The initial energy of these ions and electrons is set to 236 keV at $L = 20\ R_J$ (see Figure 9 in Wang et al., 2024).

3.1. Overview of the Evolution of Interchange Convection

Figures 2 and 3 show the typical evolution of plasma convection and concurrent energetic injection in the Jovian inner magnetosphere. Plasma motions are controlled by the competition between the electric field ($\boldsymbol{E} \times \boldsymbol{B}$) drift and the magnetic gradient/curvature (GC) drift. The latter one dominates in the inner regions closer to the planet, as demonstrated in Wang et al. (2024). Similar to Wang et al. (2023, 2024), magnetospheric evolution undergoes three stages: accumulation (Stage 1), developing (Stage 2) and quasi-steady stage (Stage 3), as illustrated in Figures 3c, 3f, and 3i. However, the evolution of plasma convection exhibits pronounced longitudinal asymmetry due to the asymmetric distribution of J_φ, as discussed in Section 2.2.

Specifically, at Stage 1 (see $T = 4$ hr in Figures 2a and 3a–3c), iogenic cold O^+ accumulates over time with a uniform longitudinally distribution within the Io torus region, corotating with Jupiter (i.e., $\omega = 0$) and having zero radial velocity Vr. During this stage, energetic particles remain stationary in Jupiter's corotating frame outside of $L = 20\ R_J$ as prescribed by the model. At $T = \sim 29$ hr, the interchange instability is then triggered after sufficient accumulation of cold plasma. The cold O^+ ions (energetic particles) are transported outward (inward) in the form of elongated fingers, displaying a significant asymmetry in longitude. As one can see in Figure 3c, the instability at longitudes with stronger J_φ (i.e., [90°, 270°]) starts to develop 5 hr earlier than that at longitudes with weaker J_φ (i.e., [−90°, 90°]). The Vr, $|\omega|$ and the mass flux are highly enhanced during this stage (Stage 2). As shown in Figure 3, since the instability grows more rapidly in the longitude sector [−90°, 90°], values of Vr, $|\omega|$ and the mass flux sampled at $T = 29$ hr are much greater than those in the sector [90°, 270°]. Finally, at stage 3, the cold O^+ outflow and energetic particle injection tend to reach a quasi-steady state, in which the statistical quantities remain steady, although the η distribution changes dramatically. As evident in Figures 2, 3b, 3e, and 3h, during Stages 2 and 3, the ω and η of particles with different energies and species exhibits a dispersion signature,

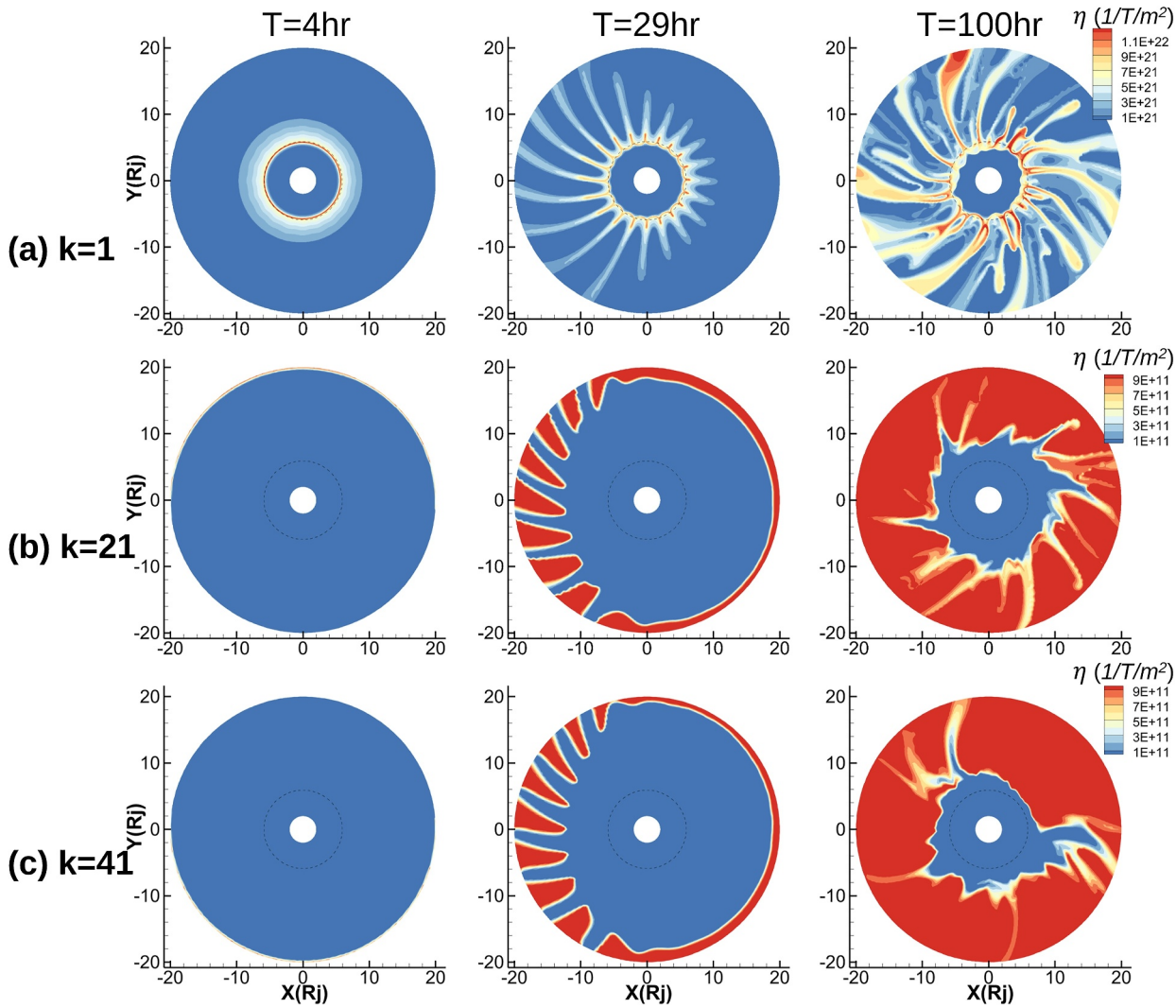

Figure 2. Equatorial distribution of η from run 5 at different times for three species: (a) cold O^+ ($k = 1$), (b) high-energy O^+ ($k = 21$) and (c) high-energy electrons ($k = 41$). The dashed black circle indicates Io's orbit of $L = 5.9\ R_J$.

particularly in inner regions where the GC drift dominates. Interestingly, at the quasi-steady stage (Stage 3), both the mass flux (Figures 3c, 3f, and 3i) and the η distribution (Figure 2, third column) exhibit little asymmetry, despite the asymmetric J_φ distribution. In other words, during the quasi-steady stage, the plasma convection of cold O^+ is mainly governed by the balance between the plasma source from Io and the losses resulting from outward transport.

3.2. Effects of the Magnetic Field Configuration on Plasma Convection

3.2.1. Intensity of Magnetodisc J_φ

The averaged J_φ is approximated by $\mu_0 I_0/2 = 139.6$ nT in the era of Juno, with variations ranging from ~120 to 160 nT across different Juno orbits (Connerney et al., 2020). As illustrated in Figure 4, the magnetic field lines passing through the same equatorial locations exhibit greater radial stretching at higher values of J_φ. The local equatorial magnetic field strength is lower with increasing J_φ, and this effect becomes more pronounced at greater distances from Jupiter. In contrast, the flux tube volume V remains almost unchanged by variations in J_φ throughout the entire inner magnetosphere.

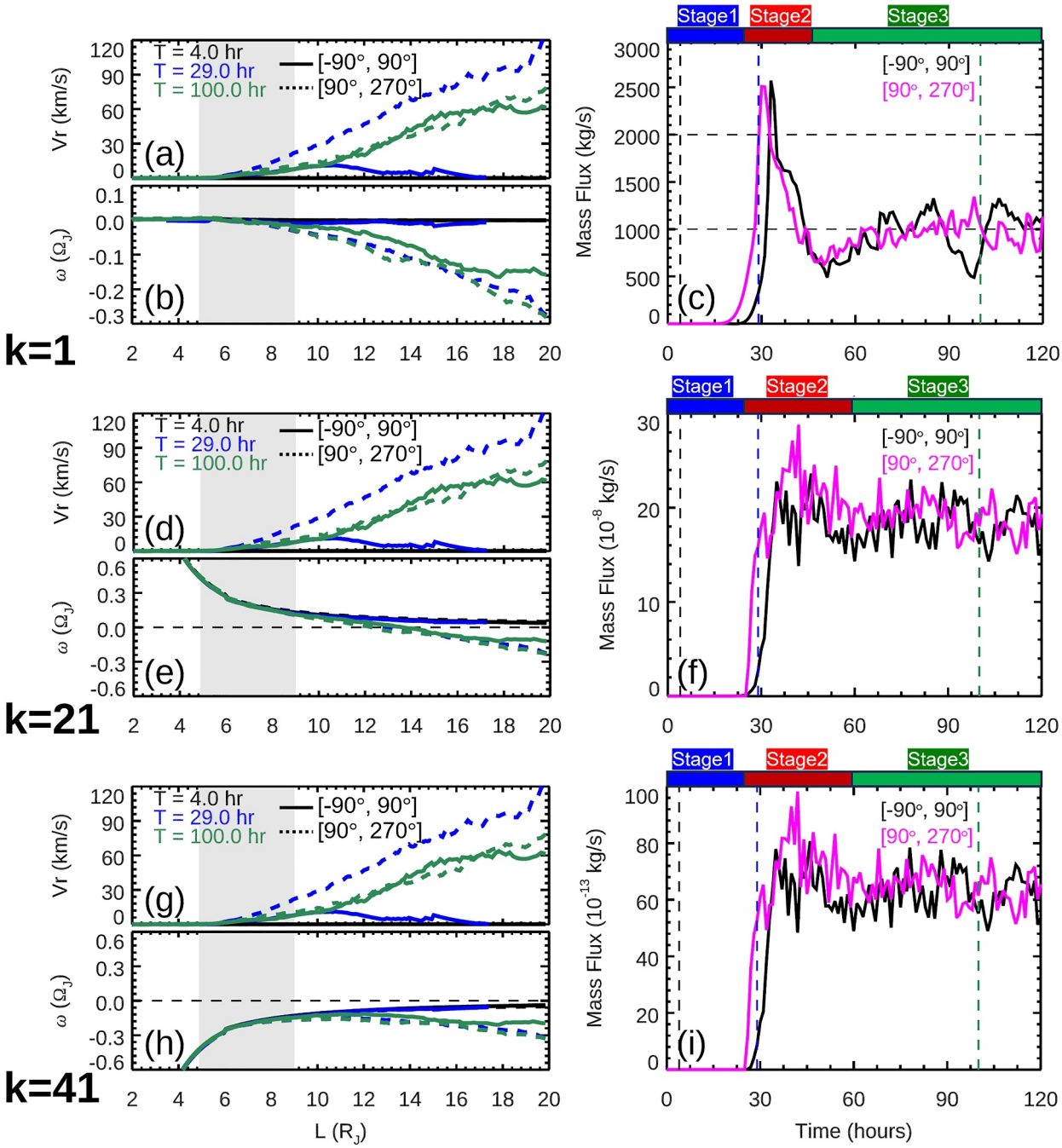

Figure 3. Evolution of plasma convection and injection from run 5 for different species as follows: (a)–(c) cold O^+ (k = 1), (d)–(f) high-energy O^+ (k = 21), and (g)–(i) high-energy electrons (k = 41). (a, d, and g) Longitude-averaged outward radial velocity Vr at three sampled times as a function of L for longitudes ranging from −90° to 90° (solid line) and from 90° to 270° (dashed line). Note that the radial velocities at T = 4.0 hr are almost zero (black curves) and coincide with the X-axis. (b, e, and h) Longitude-averaged angular velocity ω as a function of L. The gray shading denotes the Io torus region. (c, f, and i) The outflow (inflow) mass flux sampled at L = 10 R_J (19 R_J) for cold O^+ (high-energy particles) as a function of time for longitudes ranging from −90° to 90° (black) and from 90° to 270° (magenta). The three vertical dashed lines indicate the corresponding sampling times in panels (a–b, d–e and g–h). The horizontal black dashed line represents the half Io source rate adopted in the simulation.

Figure 5 presents the results of cold O^+ from runs 1–4 with different J_φ intensities (Table 1). Note that all these runs used a J_φ that is uniformly distributed in longitude. Run 2, with an intensity of 150 nT, may represent a more realistic scenario in the Jovian inner magnetosphere. At Stage 2 (T = 20–60 hr), the interchange instability

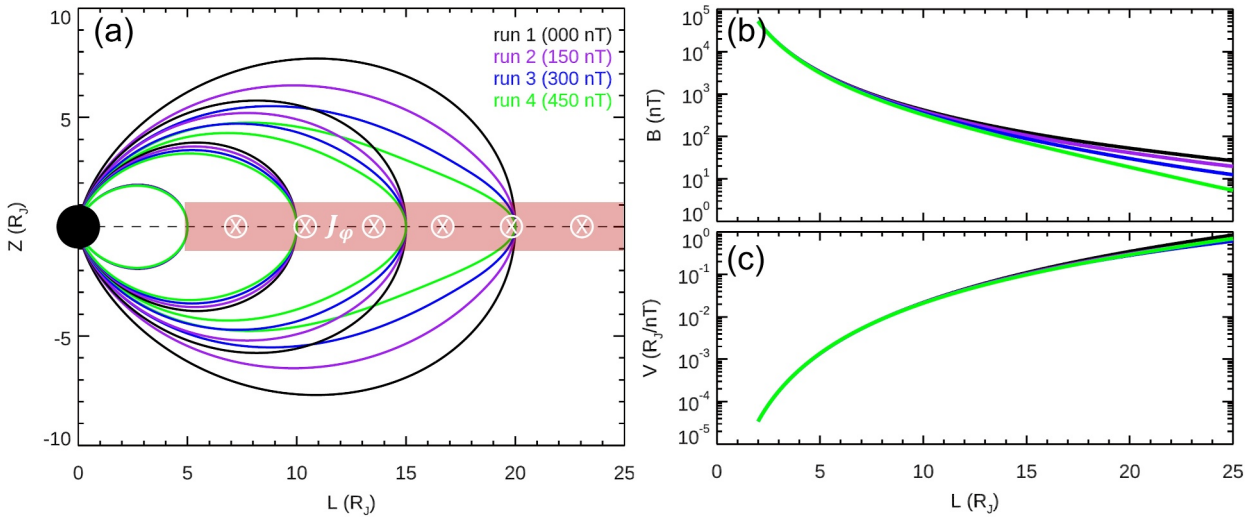

Figure 4. The magnetic field configuration for runs 1–4 with different J_φ intensities (different colors). (a) The sampled magnetic field lines in the meridian plane. The pink shading indicates the current sheet. (b and c) The equatorial magnetic field strength B and flux tube volume V as a function of L.

initiates earlier with a stronger J_φ, and the corresponding peak Vr is also higher. At Stage 3, Vr tends to increase with J_φ. The peak ω is higher for a stronger J_φ, whereas the values of ω at the quasi-steady stage remain similar. The peak mass flux sampled at $L = 10R_J$ is lower for a stronger J_φ, due to shorter accumulation time and less accumulated iogenic O^+ mass. Similar to the results from run 5 in Section 3.1, the mass flux at the quasi-steady stage remains consistent across different runs.

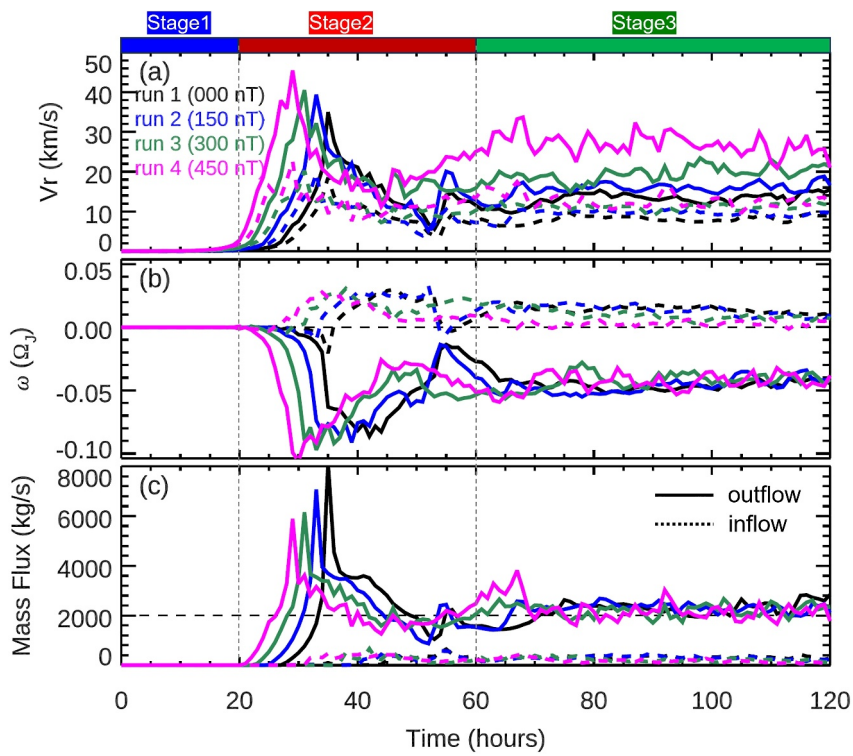

Figure 5. Evolution of cold plasma convection from runs 1–4 with different J_φ intensities as a function of time. (a) Longitude-averaged Vr for the outflow (solid) and the inflow (dashed). (b) Longitude-averaged ω. (c) The mass flux sampled at $L = 10$ R_J. The horizontal dashed line represents the Io source rate employed in the simulation.

Table 1
Model Settings for Simulation Runs of This Study

Runs	$\mu_0 I_0$ (nT)	θ_{tilt} (°)
1	0	0
2	150	0
3	300	0
4	450	0
5	50–250	0
6	100–200	0
7	0	10.25

3.2.2. Longitude Asymmetry of Magnetodisc J_φ

As detailed in Section 3.1, the asymmetric distribution of J_φ results in a longitudinally asymmetric evolution of plasma convection and energetic injection. To investigate the effect of different J_φ distributions on the convection system, runs 5 and 6 were conducted with varying distributions, compared to run 2 which uses a symmetric J_φ distribution in longitude. All runs employ the same average J_φ intensity of 150 nT.

Figure 6 illustrates the temporal evolution of the longitude-averaged Vr, ω and mass flux sampled at $L = 10\ R_J$. As expected, the instability starts in the order of run 5, run 6 and run 2, due to their increasing minimum J_φ values. The overall evolution of the longitude-averaged plasma convection, particularly during the quasi-steady stage, is similar across different distributions of J_φ intensity.

As shown in Figure 7, the evolution of the outward mass flux at different longitudes is significantly influenced by the distribution of J_φ intensity. The asymmetry of the mass flux near $T = 35$ hr becomes more pronounced with a stronger asymmetry in J_φ intensity, specifically in the order run 5> run 6> run 2. Furthermore, the mass flux in the longitude sector [0, 180°] is significantly higher than that in the sector [180°, 360°]. This longitudinal disparity can be attributed to the westward bending of the asymmetric, outward-elongated fingers due to Coriolis effects (see the second column in Figure 2a). After sufficient evolution time, the plasma convection during the quasi-steady stage shows no clear longitudinal asymmetry.

3.2.3. Intensity of Magnetodisc J_r

As mentioned in Section 2, the real Jovian magnetodisc includes a minor contribution from radial current J_r, with an intensity of $I_R = 16.7$ MA. Figure 8 illustrates the magnetic field configuration for J_r with intensities ranging from 0 to 20 MA. As depicted in Figures 3a and 3b, the direct effect of J_r is to cause the magnetic field lines to

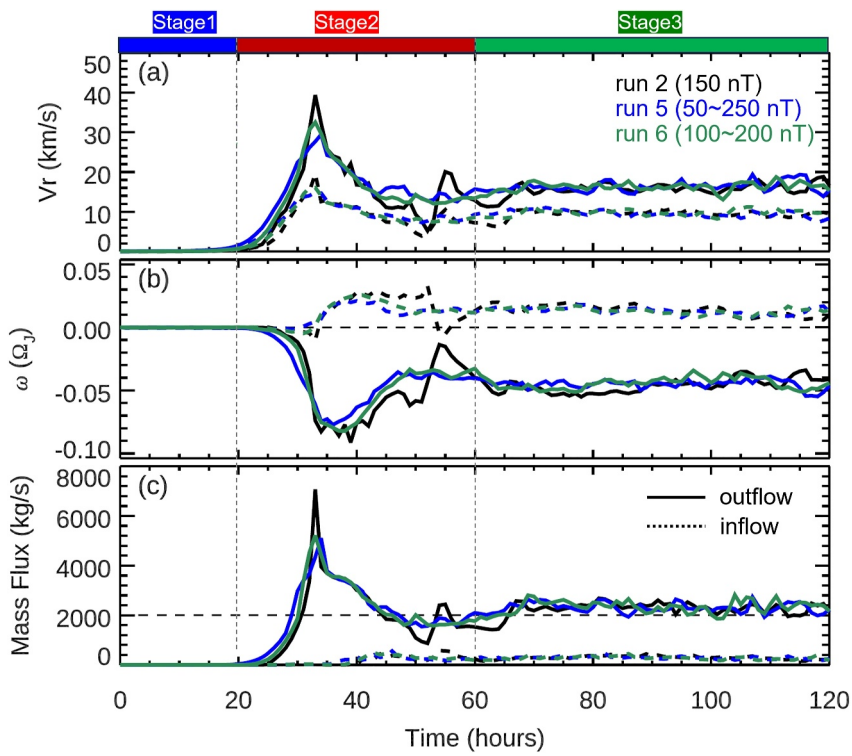

Figure 6. Same format as Figure 5, but for results from runs 2, 5, and 6 with different longitudinal distributions of J_φ.

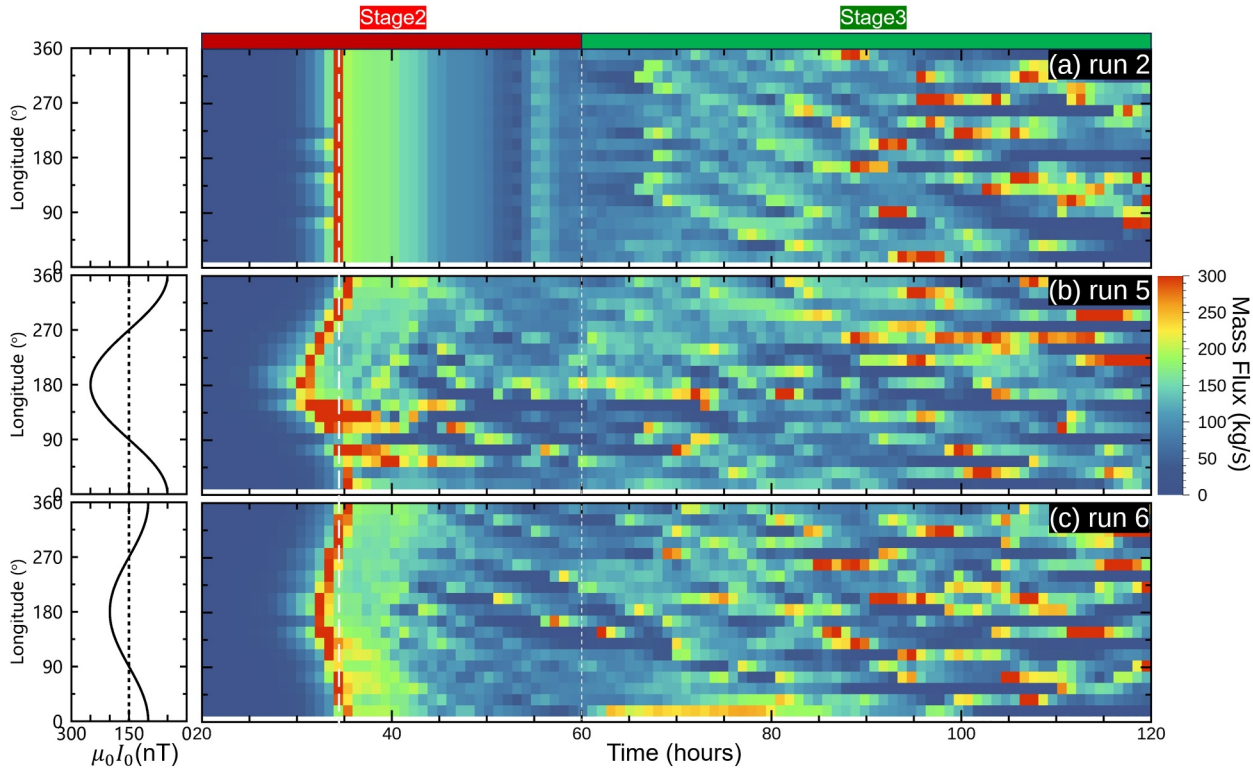

Figure 7. Temporal evolution of outward mass flux of cold O^+ at different longitudes sampled at $L = 10\ R_J$ from runs 2 (a), 5 (b) and 6 (c). The left panels show the corresponding longitude distribution of J_φ. The vertical white dashed line indicates the time when the instability develops in run 2. Note that the plot is zoomed in, starting at $T = 20$ hr, that is, the beginning of stage 2, to provide a detailed view of the evolution during stages 2 and 3.

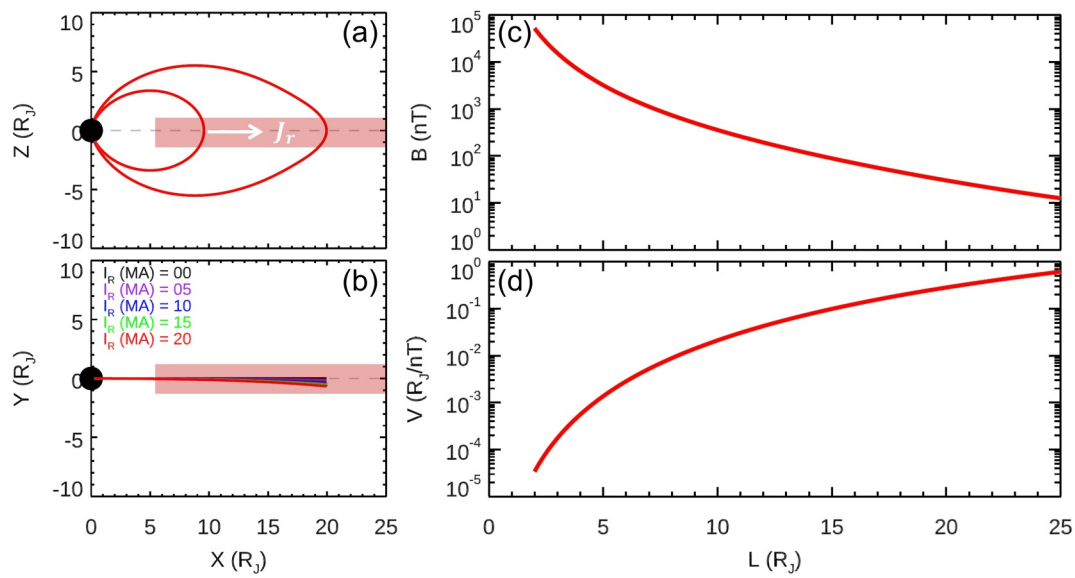

Figure 8. The magnetic field configuration with different J_r intensities (different colors). The sampled magnetic field lines in the XZ plane (a) and in the XY plane (b). The pink shading indicates the current sheet. (c) and (d) The magnetic field strength B and flux tube volume V as a function of L. Note that the magnetic field lines (a), B (c) and V (d) are almost identical for different J_r and therefore coincide with each other.

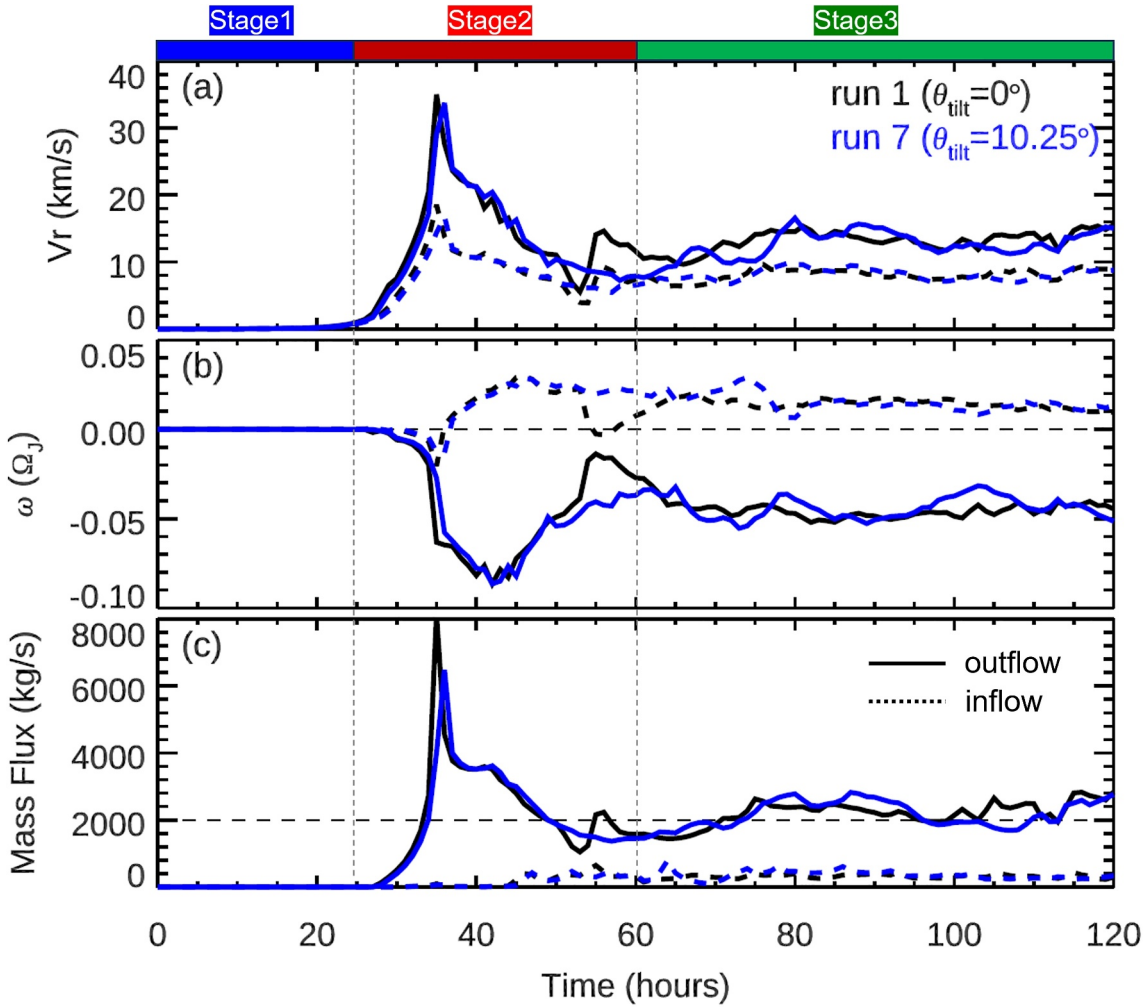

Figure 9. Same format as Figure 5, but for results from runs 1 and 7 with different magnetic tilt angles θ_{tilt}.

bend in a retrograde direction. This bending becomes more pronounced with an increasing distance from Jupiter and a stronger J_r. However, the local magnetic field B and the flux tube volume V, both crucial for the RCM simulation, remain almost identical for different values of J_r within the range of intensities considered in this study. As a result, J_r has little effect on the simulated convection in the Jovian inner magnetosphere (not shown in the paper).

3.2.4. Magnetic Tilt Angle θ_{tilt}

Figure 9 presents the results from run 1 and run 7, illustrating the effect of a magnetic tilt angle on the plasma convection. As described in Section 2.2, introducing a tilt angle effectively reduces the angular velocity to $\Omega_J \cdot \cos(\theta_{tilt})$, i.e., 0.984 Ω_J. As one can see in Figure 9, the general evolution of the plasma convection and the associated plasma flow are almost the same for these two runs. However, as expected, run 7 shows a slightly smaller peak radial velocity Vr and mass flux for the outflow, as a result of its reduced angular velocity relative to run 1. Furthermore, the onset of the interchange instability occurs earlier in run 1 than in run 7.

4. Discussion

4.1. Analysis of J_φ Effects on the Convection

The linear growth rate γ of the interchange instability is proportional to flux tube content η, and inversely proportional to the equatorial magnetic field B, as demonstrated by both linear theories (e.g., Huang & Hill, 1991;

Pontius, 1997; Vasyliūnas & Pontius, 2007) and numerical simulations (e.g., Wang et al., 2023, 2024; Yang et al., 1994). As shown in Figure 4, B decreases with increasing J_φ. Consequently, the Io source rate per unit magnetic flux $\dot{\eta} = \dot{N}/B$ increases for a given source rate per unit equatorial area $\dot{N}$ ($m^{-2}s^{-1}$) (see Equation 6 in Wang et al., 2023). This results in a higher value of $\eta = \dot{\eta}\Delta t$ during the same time period Δt. Therefore, a higher η and a smaller B for strong J_φ lead to a higher growth rate γ. This is consistent with the simulation results presented in Section 3.2.

4.2. Comparison With Observations

In our previous RCM simulations using a spin-aligned dipole magnetic field (Wang et al., 2023, 2024), the simulated Vr is much larger than that observed, while the modeled ω of the outflow and the number density are much smaller than Galileo data.

As described in Section 3, the magnetic field configuration can significantly influence plasma convection in the Jovian inner magnetosphere. Specifically, Vr during the quasi-steady stage tends to increase with increasing J_φ. Therefore, an enhanced J_φ exacerbates the discrepancy between simulation results and observations. The modeled ω of the plasma outflow remains much smaller than observations, although it does slightly increase for stronger J_φ. Furthermore, the simulated number density appears largely unaffected by changes in the magnetic field configuration (not shown in the paper). These findings suggest that employing a more realistic magnetic field configuration, derived from static models such as JRM33 (Connerney et al., 2022) and CON20 (Connerney et al., 2020), does not reduce the discrepancies between simulation results and observations. Such disparities may arise from the unrealistic representation of the Io torus, energetic particles and ionospheric conductances, which should be investigated in future studies.

As outlined in Section 3.2, changes in J_φ intensity and its longitudinal asymmetry significantly impact interchange convection. This may suggest that factors such as a sudden solar wind pressure pulse can alter J_φ, thereby modulating plasma transport in Jupiter's inner magnetosphere. Notably, although the effect of J_φ longitudinal asymmetry becomes less pronounced during the quasi-steady stage, plasma convection in a real magnetosphere remains substantially influenced by the magnetic field for two reasons: (a) Jupiter's magnetosphere is highly dynamic over time, making the quasi-steady state hard to achieve, and (b) local time (longitude) asymmetry, especially dawn-dusk and day-night asymmetry, remains almost fixed in the inertial frame rather than corotating with Jupiter. This contrasts with our model's assumption of a magnetic field that corotates with Jupiter.

4.3. Directions for Future Work

In this study, we focus on the effect of magnetic field configuration on interchange convection in the Jovian inner magnetosphere. The magnetic field configuration is primarily determined by the magnetodisc currents J_r and J_φ. However, in our model, this magnetic field is prescribed and remains fixed over time, unaffected by the plasma flow. This is a limitation within the RCM framework (Wang et al., 2023, 2024). To study the characteristics of magnetic field topology and its role during interchange events, future simulations should incorporate more realistic magnetic fields that are consistent with plasma flow dynamics. Such fields can be derived from a Jovian MHD model (e.g., Wang et al., 2018, 2022). The single-fluid global MHD model for the Jovian magnetosphere is capable of reproducing the 3D evolution of the interchange convection of iogenic plasma in a more consistent manner (e.g., Chen et al., 2023; Feng et al., 2023; Tanaka et al., 2023). Although energetic particles and their GC drift are not included in MHD simulations, comparisons with RCM results can enhance our understanding of plasma and energy circulation at Jupiter. Future work should also consider the effects of energetic particles (Yang et al., 1994) and incorporate a more realistic ionospheric conductance model that includes meteorite contributions (Clément et al., 2025).

5. Summary and Conclusions

In this study, we used the improved RCM-Jupiter code to simulate cold plasma convection and energetic particle injection in Jupiter's inner magnetosphere. This model employs a more realistic magnetic field based on the JRM33 (Connerney et al., 2022) and CON20 (Connerney et al., 2020) models. We conducted a series of simulations varying the intensities of magnetodisc currents J_r and J_φ, the longitudinal distribution of J_φ, and the magnetic tilt angle θ_{tilt}. Our parametric study provides insights into how these parameters influence interchange

convection at Jupiter. The findings indicate that previous simulations using a simplified magnetic dipole underestimated the interchange instability, and the absence of longitudinal asymmetry may cause discrepancies between model results and observations.

The results of this paper can be summarized as follows:

1. The overall evolution of interchange convection for both cold O^+ ions and energetic particles is generally similar across different magnetic field configurations. The magnetosphere experiences three main stages: an accumulation stage (a standby stage), a developing stage and a quasi-steady stage for cold O^+ ions (energetic particles).
2. The J_φ intensity in the magnetodisc significantly influences plasma convection. As J_φ increases, the local equatorial magnetic field strength B weakens, leading to an increase in interchange instability. This instability and the associated plasma flow initiate earlier in simulations with a strong J_φ. The peak plasma velocities Vr and ω during the accumulation stage, and Vr during the quasi-steady stage tend to increase with increasing J_φ. However, the mass flux at the quasi-steady stage remains similar and is largely unaffected by variations in J_φ intensity.
3. The longitudinal distribution of J_φ strongly modulates plasma convection during the developing stage, increasing the asymmetry in longitude observed during this stage. However, the overall longitude-averaged plasma convection, particularly during the quasi-steady stage, is similar across different distributions of J_φ intensity. Notably, the longitudinal asymmetry becomes less pronounced or disappears entirely by the quasi-steady stage.
4. The J_r intensity has little effect on plasma convection within the range of intensities observed in reality. This suggest that the overall impact of J_r is relatively small under realistic conditions in the Jovian inner magnetosphere.
5. The magnetic tilt angle θ_{tilt} relative to the rotational axis slightly decreases interchange instability by effectively reducing the planetary angular velocity. Consequently, the Vr, ω and mass flow are slightly altered.

Data Availability Statement

In this study, all simulation data and the model code are available at the Science Data Bank (Wang et al., 2025; Wang & Guo, 2025).

Acknowledgments
This work was supported by NNSFC Grants 42188101, 42304189, 42150105, the National Key R&D Program of China 2021YFA0718600, Pandeng Program of National Space Science Center, Chinese Academy of Sciences, the Climbing Program of NSSC (E4PD3001), the Pre-research Project on Civil Aerospace Technologies D010301 and D010202 funded by the China National Space Administration (CNSA), and in part by the Specialized Research Fund for State Key Laboratories of China. We are grateful to J. Yang for the helpful discussions on the simulation code.

References

Al Saati, S., Clément, N., Louis, C., Blanc, M., Wang, Y., André, N., et al. (2022). Magnetosphere-ionosphere-thermosphere coupling study at Jupiter based on Juno's first 30 orbits and modeling tools. *Journal of Geophysical Research: Space Physics*, *127*(10), e2022JA030586. https://doi.org/10.1029/2022JA030586

André, N., & Ferrière, K. M. (2007). Comments on Vasyliunas' and Pontius' studies of the effects of the planetary ionosphere and of the Coriolis force on the interchange instability: Commentary. *Journal of Geophysical Research*, *112*(A10). https://doi.org/10.1029/2006JA011732

Bagenal, F., Adriani, A., Allegrini, F., Bolton, S. J., Bonfond, B., Bunce, E. J., et al. (2017). Magnetospheric science objectives of the Juno Mission. *Space Science Reviews*, *213*(1–4), 219–287. https://doi.org/10.1007/s11214-014-0036-8

Bagenal, F., & Delamere, P. A. (2011). Flow of mass and energy in the magnetospheres of Jupiter and Saturn: Mass and energy. *Journal of Geophysical Research*, *116*(A5). https://doi.org/10.1029/2010ja016294

Bolton, S. J., Bagenal, F., Blanc, M., Cassidy, T., Chané, E., Jackman, C., et al. (2015). Jupiter's magnetosphere: Plasma sources and transport. *Space Science Reviews*, *192*(1–4), 209–236. https://doi.org/10.1007/s11214-015-0184-5

Bolton, S. J., Thorne, R. M., Gurnett, D. A., & Williams, D. J. (1997). Enhanced whistler-mode emissions: Signatures of interchange motion in the Io. *Geophysical Research Letters*, *24*(17), 2123–2126. https://doi.org/10.1029/97gl02020

Burch, J. L., Goldstein, J., Hill, T. W., Young, D. T., Crary, F. J., Coates, A. J., et al. (2005). Properties of local plasma injections in Saturn's magnetosphere: Local plasma injections at Saturn. *Geophysical Research Letters*, *32*(14). https://doi.org/10.1029/2005GL022611

Chen, J., Zhang, B., Lin, D., Delamere, P. A., Yao, Z., Brambles, O., et al. (2023). Prediction of axial asymmetry in Jovian magnetopause reconnection. *Geophysical Research Letters*, *50*(9), e2022GL102577. https://doi.org/10.1029/2022GL102577

Clément, N., Nakamura, Y., Blanc, M., Wang, Y., & Saati, S. A. (2025). Ionospheric conductances at the giant planets of the solar system: A comparative study of ionization sources and the impact of meteoric ions. https://doi.org/10.48550/arXiv.2412.04219

Connerney, J. E. P., Timmins, S., Herceg, M., & Joergensen, J. L. (2020). A Jovian magnetodisc model for the Juno Era. *Journal of Geophysical Research: Space Physics*, *125*(10), e2020JA028138. https://doi.org/10.1029/2020JA028138

Connerney, J. E. P., Timmins, S., Oliversen, R. J., Espley, J. R., Joergensen, J. L., Kotsiaros, S., et al. (2022). A new model of Jupiter's magnetic field at the completion of Juno's Prime Mission. *Journal of Geophysical Research: Planets*, *127*(2). https://doi.org/10.1029/2021je007055

Daly, A., Li, W., Ma, Q., Shen, X.-C., Capannolo, L., Huang, S., et al. (2024). Statistical survey of interchange events in the Jovian magnetosphere using Juno observations. *Geophysical Research Letters*, *51*(19), e2024GL110300. https://doi.org/10.1029/2024GL110300

Daly, A., Li, W., Ma, Q., Shen, X.-C., Yoon, P. H., Menietti, J. D., et al. (2023). Plasma wave and particle dynamics during interchange events in the Jovian magnetosphere using Juno observations. *Geophysical Research Letters*, *50*(23), e2023GL103894. https://doi.org/10.1029/2023GL103894

Dumont, M., Grodent, D., Radioti, A., Bonfond, B., & Gérard, J.-C. (2014). Jupiter's equatorward auroral features: Possible signatures of magnetospheric injections. *Journal of Geophysical Research: Space Physics*, *119*(12). https://doi.org/10.1002/2014JA020527

Dumont, M., Grodent, D., Radioti, A., Bonfond, B., Roussos, E., & Paranicas, C. (2018). Evolution of the auroral signatures of Jupiter's magnetospheric injections. *Journal of Geophysical Research: Space Physics*, *123*(10), 8489–8501. https://doi.org/10.1029/2018JA025708

Feng, E., Zhang, B., Yao, Z., Delamere, P. A., Zheng, Z., Dunn, W. R., & Ye, S. (2023). Variation of the Jovian magnetopause under constant solar wind conditions: Significance of magnetodisc dynamics. *Geophysical Research Letters*, *50*(12), e2023GL104046. https://doi.org/10.1029/2023GL104046

Grodent, D. (2015). A brief review of ultraviolet auroral emissions on giant planets. *Space Science Reviews*, *187*(1–4), 23–50. https://doi.org/10.1007/978-1-4939-3395-2_3

Grodent, D., Bonfond, B., Yao, Z., Gérard, J.-C., Radioti, A., Dumont, M., et al. (2018). Jupiter's Aurora observed with HST during Juno orbits. *Journal of Geophysical Research: Space Physics*, *123*(5), 3299–3319. https://doi.org/10.1002/2017ja025046

Haggerty, D. K., Mauk, B. H., Paranicas, C. P., Clark, G., Kollmann, P., Rymer, A. M., et al. (2019). Jovian injections observed at high latitude. *Geophysical Research Letters*, *46*(16), 9397–9404. https://doi.org/10.1029/2019GL083442

Huang, T. S., & Hill, T. W. (1991). Drift wave instability in the Io plasma torus. *Journal of Geophysical Research*, *96*(A8), 14075–14083. https://doi.org/10.1029/91JA01170

Khurana, K. K. (2001). Influence of solar wind on Jupiter's magnetosphere deduced from currents in the equatorial plane. *Journal of Geophysical Research*, *106*(A11), 25999–26016. https://doi.org/10.1029/2000JA000352

Kivelson, M. G., Khurana, K. K., Russell, C. T., & Walker, R. J. (1997). Intermittent short-duration magnetic field anomalies in the Io torus: Evidence for plasma interchange? *Geophysical Research Letters*, *24*(17), 2127–2130. https://doi.org/10.1029/97gl02202

Krupp, N., Vasyliunas, V. M., Woch, J., Lagg, A., Khurana, K. K., Kivelson, M. G., et al. (2004). Dynamics of the Jovian magnetosphere. In F. Bagenal, T. E. Dowling, & W. B. Mckinnon (Eds.), *Jupiter. The planet, satellites and magnetosphere* (pp. 617–638). Cambridge University Press.

Krupp, N., Woch, J., Lagg, A., Roelof, E. C., Williams, D. J., Livi, S., & Wilken, B. (2001). Local time asymmetry of energetic ion anisotropies in the Jovian magnetosphere. *Planetary and Space Science*, *49*(3–4), 283–289. https://doi.org/10.1016/S0032-0633(00)00149-5

Liu, X., & Hill, T. W. (2012). Effects of finite plasma pressure on centrifugally driven convection in Saturn's inner magnetosphere: Effects of plasma pressure on convection. *Journal of Geophysical Research*, *117*(A7). https://doi.org/10.1029/2012ja017827

Liu, Z.-Y., Blanc, M., Andre, N., Bagenal, F., Wilson, R. J., Allegrini, F., et al. (2024). Juno observations of Jupiter's Magnetodisk plasma: Implications for equilibrium and dynamics. *Journal of Geophysical Research: Space Physics*, *129*(11), e2024JA032976. https://doi.org/10.1029/2024JA032976

Liu, Z.-Y., Blanc, M., & Zong, Q.-G. (2023). A Juno-Era view of electric currents in Jupiter's magnetodisk. *Journal of Geophysical Research: Space Physics*, *128*(10), e2023JA031436. https://doi.org/10.1029/2023JA031436

Louarn, P., Paranicas, C. P., & Kurth, W. S. (2014). Global magnetodisk disturbances and energetic particle injections at Jupiter: Global disturbances of Jovian disk. *Journal of Geophysical Research: Space Physics*, *119*(6), 4495–4511. https://doi.org/10.1002/2014ja019846

Mauk, B. H., Clarke, J. T., Grodent, D., Waite, J. H., Paranicas, C. P., & Williams, D. J. (2002). Transient aurora on Jupiter from injections of magnetospheric electrons. *Nature*, *415*(6875), 1003–1005. https://doi.org/10.1038/4151003a

Mauk, B. H., Williams, D. J., & McEntire, R. W. (1997). Energy-time dispersed charged particle signatures of dynamic injections in Jupiter's inner magnetosphere. *Geophysical Research Letters*, *24*(23), 2949–2952. https://doi.org/10.1029/97GL03026

Menietti, J. D., Santolik, O., Rymer, A. M., Hospodarsky, G. B., Persoon, A. M., Gurnett, D. A., et al. (2008). Analysis of plasma waves observed within local plasma injections seen in Saturn's magnetosphere: Waves in Saturn's plasma injections. *Journal of Geophysical Research*, *113*(A5). https://doi.org/10.1029/2007JA012856

Moncuquet, M., Bagenal, F., & Meyer-Vernet, N. (2002). Latitudinal structure of outer Io plasma torus. *Journal of Geophysical Research*, *107*(A9), 1260. https://doi.org/10.1029/2001JA900124

Phipps, P., & Bagenal, F. (2021). Centrifugal equator in Jupiter's plasma sheet. *Journal of Geophysical Research: Space Physics*, *126*(1). https://doi.org/10.1029/2020JA028713

Pontius, D. H. (1997). Coriolis influences on the interchange instability. *Geophysical Research Letters*, *24*(23), 2961–2964. https://doi.org/10.1029/97GL53157

Radioti, A., Grodent, D., Gérard, J.-C., Roussos, E., Paranicas, C., Bonfond, B., et al. (2009). Transient auroral features at Saturn: Signatures of energetic particle injections in the magnetosphere: Transient aurora at Saturn. *Journal of Geophysical Research*, *114*(A3). https://doi.org/10.1029/2008JA013632

Schok, A. A., Delamere, P. A., Mino, B., Damiano, P. A., Zhang, B., Sciola, A., et al. (2023). Periodicities and plasma density structure of Jupiter's dawnside magnetosphere. *Journal of Geophysical Research: Planets*, *128*(2), e2022JE007637. https://doi.org/10.1029/2022JE007637

Southwood, D. J., & Kivelson, M. G. (1989). Magnetospheric interchange motions. *Journal of Geophysical Research*, *94*(A1), 299–308. https://doi.org/10.1029/JA094iA01p00299

Tanaka, T., Ebihara, Y., Watanabe, M., Fujita, S., & Kataoka, R. (2023). Radial transport of Io plasma from the inner magnetosphere to the tail. *Journal of Geophysical Research: Space Physics*, *128*(5), e2022JA030891. https://doi.org/10.1029/2022JA030891

Toffoletto, F., Sazykin, S., Spiro, R., & Wolf, R. (2003). Inner magnetospheric modeling with the rice convection model. In A. C.-L. Chian, I. H. Cairns, S. B. Gabriel, J. P. Goedbloed, T. Hada, M. Leubner, et al. (Eds.), *Advances in space environment research - Volume I* (pp. 175–196). Springer Netherlands. https://doi.org/10.1007/978-94-007-1069-6_19

Vasyliunas, V. M. (1983). *Plasma distribution and flow*. Cambridge University Press.

Vasyliūnas, V. M., & Pontius, D. H. (2007). Rotationally driven interchange instability: Reply to André and Ferrière. *Journal of Geophysical Research*, *112*(A10). https://doi.org/10.1029/2007JA012457

Wang, Y., Blanc, M., Louis, C., Wang, C., André, N., Adriani, A., et al. (2021). A preliminary study of magnetosphere-ionosphere-thermosphere coupling at Jupiter: Juno multi-instrument measurements and modeling tools. *Journal of Geophysical Research: Space Physics*, *126*(9), e2021JA029469. https://doi.org/10.1029/2021ja029469

Wang, Y., & Guo, X. (2025). Simulation code of "Effect of Magnetic Field Configuration on Interchange Convection in Jovian Inner Magnetosphere" (version V1) [Dataset]. *Science Data Bank*. https://doi.org/10.57760/sciencedb.space.02455

Wang, Y., Guo, X., Blanc, M., Li, H., & Wang, C. (2025). Simulation data of "Effect of Magnetic Field Configuration on Interchange Convection in Jovian Inner Magnetosphere" (version V1) [Dataset]. *Science Data Bank*. https://doi.org/10.57760/sciencedb.space.02370

Wang, Y., Guo, X., Tang, B., Li, W., & Wang, C. (2018). Modeling the Jovian magnetosphere under an antiparallel interplanetary magnetic field from a global MHD simulation. *Earth and Planetary Physics*, *2*(4), 303–309. https://doi.org/10.26464/epp2018028

Wang, Y., Guo, X., Wang, C., & Blanc, M. (2022). Response of the Jovian magnetosphere-ionosphere system to the interplanetary magnetic field discontinuity: A simulation study. *Journal of Geophysical Research: Space Physics*, *127*(6). https://doi.org/10.1029/2021JA030207

Wang, Y., Yang, J., Guo, X., Blanc, M., & Wang, C. (2024). Energetic plasma injections in Jovian inner magnetosphere: A simulation study. *Journal of Geophysical Research: Planets*, *129*(2). https://doi.org/10.1029/2023JE008178

Wang, Y., Yang, J., Guo, X., Wang, C., & Blanc, M. (2023). Simulation of centrifugally driven convection in Jovian inner magnetosphere using the rice convection model. *Journal of Geophysical Research: Space Physics*, *128*(3). https://doi.org/10.1029/2022JA031132

Wilson, R. J., Vogt, M. F., Provan, G., Kamran, A., James, M. K., Brennan, M., & Cowley, S. W. H. (2023). Internal and external Jovian magnetic fields: Community code to serve the magnetospheres of the outer planets community. *Space Science Reviews*, *219*(1), 15. https://doi.org/10.1007/s11214-023-00961-3

Wu, H., Hill, T. W., Wolf, R. A., & Spiro, R. W. (2007). Numerical simulation of fine structure in the Io plasma torus produced by the centrifugal interchange instability: Fine structure of Io plasma torus. *Journal of Geophysical Research*, *112*(A2). https://doi.org/10.1029/2006JA012032

Yang, Y. S., Wolf, R. A., Spiro, R. W., Hill, T. W., & Dessler, A. J. (1994). Numerical simulation of torus-driven plasma transport in the Jovian magnetosphere. *Journal of Geophysical Research*, *99*(A5), 8755–8770. https://doi.org/10.1029/94ja00142

Yao, Z. H., Bonfond, B., Clark, G., Grodent, D., Dunn, W. R., Vogt, M. F., et al. (2020). Reconnection- and dipolarization-driven auroral dawn storms and injections. *Journal of Geophysical Research: Space Physics*, *125*(8). https://doi.org/10.1029/2019JA027663

Yin, Z., Ren, Z., Zhou, X., Sun, Y., Ye, S., Duanmu, X., et al. (2025). Particle-trapping injection flux tubes in Saturn's magnetosphere and high-band electron cyclotron harmonic waves therein. *Geophysical Research Letters*, *52*(3), e2024GL113094. https://doi.org/10.1029/2024GL113094

Yuan, C., Roussos, E., Wei, Y., Krupp, N., Liu, Z., & Wang, J. (2024). Galileo observation of electron spectra dawn-dusk asymmetry in the Middle Jovian magnetosphere: Evidence for convection electric field. *Geophysical Research Letters*, *51*(1), e2023GL105503. https://doi.org/10.1029/2023GL105503